Advances in Engineering Science
Online access @ www.publishingindia.com

POLYANILINE AND POLYPYROLE AS CATHODE MATERIALS FOR ZINC BATTERIES IN CHLORIDE AND CHLORIDE/CITRATE BASED ELECTROLYTES

Branimir N. Grgur*

Faculty of Technology and Metallurgy, Karnegijeva 4
11000 Belgrade, Serbia and Montenegro

ABSTRACT

Electrochemical behavior of zinc, thin polyaniline (PANI) and polypyrole (PPy) electrode polymerized from 0.1 M HCl and 0.1 M aniline or 0.1 M pyrole on graphite electrode, in 0.2 M $ZnCl_2$ and 0.50 M NH_4Cl (**chloride electrolyte**) and with addition of 0.33 M Na-citrate (**chloride/citrate electrolyte**) were investigated. In the range of investigated charge/discharge current densities of 0.25 to 1 mA cm^{-2}, initially obtained specific capacity of PANI electrode was in the range of 140 to 85 mAh g^{-1}, respectively. Specific capacity and columbic efficiency were affected with anodic potential limits. For anodic potential limits of 0.32 V (SCE) citrate/chloride electrolyte shows better characteristic than chloride electrolyte, due to the influence of citrate ions on negative shift of doping reaction. Increasing anodic potential limit to 0.5 V (SCE), leads to faster decrease of specific capacity in citrate/ chloride than in chloride electrolyte, which was explained by higher hydrophilic effect of citrate anions. PPy electrode shows similar charge/discharge characteristics in chloride and in chloride/citrate electrolyte. In the range of investigated current densities of 0.1 to 0.75 mA cm^{-2}, discharge electrode capacity was in the range of 0.075 to 0.045 mA h cm^{-2} or 100 to 60 mA h g^{-1}, respectively. For the same synthesis and operating conditions PANI electrode shows much better electrochemical characteristic than PPy electrode. In the chloride/citrate comparing with chloride containing electrolyte zinc electrode shows negative shift of the open circuit potential of ~130 mV, decreases of exchange current density for more than order of magnitude and increase of cathodic Tafel slope, due to the zinc ions complexation. In citrate/chloride electrolyte zinc dendrite formation were suppressed.

Key words: polyaniline, polypyrole, zinc batteries, chloride citrates, dendrites

1. INTRODUCTION

The electrochemical properties of polyaniline and polypyrole films due to their low specific weight when compared with classical inorganic compounds; high energy and power density and ability to reversible exchange counter ions, have stimulated the interest in their use as electrode materials of secondary batteries. A first attempt to develop a secondary cell with a PAN1 film and an aqueous electrolyte was made by de Surville et al. [1], while Kitani et al. reported the first water based Zn–PANI rechargeable battery [2, 3]. Zinc-polyaniline secondary cells have some advantages, in comparison with classical (protonic and aprotonic) battery types like ecological acceptability, uses of water based electrolytes (mainly ammonium/zinc chloride) [4, 5] and relatively low price. A Zn|$ZnCl_2$, NH_4Cl|PANI, porous carbon cell described by Trinidad et al. [6] showed similar electrochemical characteristics to those of conventional batteries, i.e., moderate energy density (50-100 Wh kg^{-1}), good columbic efficiency (70-100%), low self-discharge rate and long cycle life.

Up to now zinc-PANI batteries has not been commercialized from few reasons. First reason is degradation process of PANI electrode at potentials more positive than ~0.5 V [7, 8]. In chloride containing electrolytes Zn electrodes form dendrites during charge–discharge cycles [9, 10], which results in decreased columbic efficiency and cycle life. Main reason for that are sort circuit provoked by penetration of dendrites through separator to cathode or formation of the anodic slime. On the

*bngrgur@tmf.bg.ac.yu

other hand during cyclization zinc passivation occur, which is possibly related to the formation of the solid phases, $ZnCl_2 \cdot 3NH_4Cl$ and $ZnCl_2 \cdot 2NH_4Cl$, on the anode surface [11].

It is interesting to mention that up to now PPy electrode were not investigated as possible cathode materials for application in zinc batteries. It is well known that some organic anions form complexes with the metal ions, that results much better quality of the metal deposits and suppress dendrite formation [12]. Probably, the best choice will be oxalic anions, due to the small ionic radius, good PANI and PPy doping-dedoping characteristics, etc [13]. Unfortunately, zinc oxalate is a low soluble salt. In this paper we investigated behavior of zinc, PANI and PPy electrodes in chloride containing electrolytes and with addition of citrate anions, which at pH~5 form an soluble zinc citrate $[ZnCit]^-$ complex with pK_s value of 4.8.

2. EXPERIMENTAL

Polyaniline and polypyrole thin film electrode was obtained from hydrochloric acid solution (0.1 M) with addition of 0.1 M aniline or 0.1 M of pyrole monomer (p.a. Merck, distilled in argon atmosphere), at constant current densities of 2 mA cm^{-2} on graphite electrode. Electrolytes containing 0.5 M NH_4Cl, 0.20 M $ZnCl_2$ and with addition of 0.33 M sodium citrate were prepared from p.a. grade chemicals (Merck) and bidistiled water. pH of the electrolytes in all experiments was 5. For all experiments three compartment electrochemical cell, with platinum foil (S=2 cm^2) as a counter and saturated calomel electrode, E_r=0.243 V (SHE) as a reference electrode at room temperature (22^{0}C) was used.

The working electrodes, cylindrically shaped graphite inserted in Teflon holder (S=0.64 cm^2) were mechanically polished with fine emery papers (2/0, 3/0 and 4/0, respectively) and then with polishing alumina of 1 mm (Banner Scientific Ltd.) on the polishing cloths (Buehler Ltd.). After mechanical polishing the traces of polishing alumina were removed from the electrode surface in an ultra-sonic bath in ethanol during 5 min. The electrochemical measurements were carried using a PAR 273A potentiostat controlled by a computer through a GPBI PC2A interface.

Micrographs of the zinc deposits obtained on the copper substrate (4 cm^2) at the current density of 3.5 mA cm^{-2} are taken with optical microscope connected with computer

3. RESULTS AND DISCUSSION

3.1. Synthesis and characterization of the polymer electrode

Figure 1 shows the galvanostatic curve for polymerization of aniline and pyrole from solution containing 0.10 M HCl and 0.10 M monomer on graphite electrode at current density of 2 mA cm^{-2} with polymerization charge of 0.6 mA h cm^{-2} (1080s) respectively.

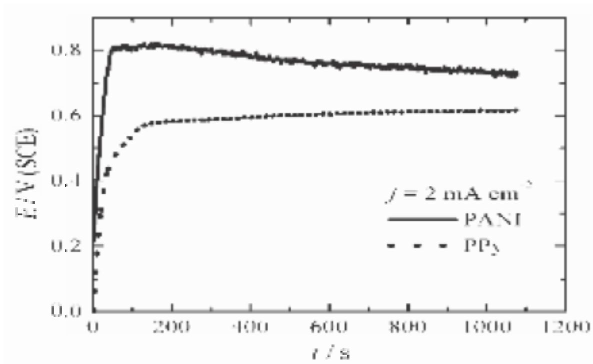

Figure 1 : Galvanostatic curve for (——) aniline and (--------) pyrole polymerization from 0.1 M HCl and 0.1 M monomere at 2 mA cm^{-2} on graphite electrode.

Polymerization of PANI proceed in the potential range between 0.8 and 0.75 V, while polymerization of PPy at ~0.6 V. Assuming 100% current efficiency during the polymerization and using equation [14, 15]:

$$m = \frac{jt\left(M_m + yM_a\right)}{(2+y)F} \quad (1)$$

where m, g, is the mass of the polymer polymerized with current density j, A cm^{-2}, during the time, t, s, M_m and M_a, g mol^{-1}, are molar mass of the polymer monomer and inserted, chlorine, anions, F = 96500 A s mol^{-1} is Faraday constant, and y is is doping degree. For the different PANI oxidation states (emeraldine salt, y=0.5 and perningemeraldine y=1) which can be expected for polymerization potentials of ~0.75 V, it could be calculated that mass of the PANI on graphite electrode is approximately 1 mg cm^{-2} for applied polymerization current density of 2 mA cm^{-2} and for polymerization time of 1080 s. But, due to the high polymerization potentials it should be suggested that after polymerization PANI was in pernigemeraldine state (y=1).

For the same synthesis conditions and for the theoretical doping degree of y = 0.25 for the PPy electrode it can be calculated mass of the 0.75 mg cm^{-2}.

After polymerization, electrodes were washed with bidistiled water and transferred in the three compartment electrochemical cell with chloride or chloride/citrate electrolyte. After transfer, electrode was conditioned at potential of –0.8 V for 600 s to be completely discharged and cyclic voltammograms were taken.

Figure 2 shows the cyclic voltammograms of the PANI electrode in different electrolytes. Graphite electrode in the investigated potential range do not shows any features which could be connected with oxidation or reduction of citrate anions, so redox processes can be attributed to reaction of the PANI film.

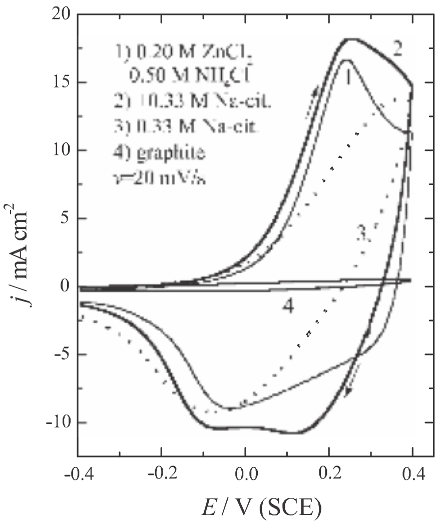

Figure 2 : Comparison of cyclic voltammograms (20 mV s^{-1}) of PANI electrode in 1) chloride, 2) chloride/citrate 3) pure citrate electrolyte and 4) for the bare graphite electrode.

In chloride electrolyte, anodic peak at ~0.1 V is well pronounced, while in chloride/citrate electrolyte it seams that peak is overlapped with contributions of some other reaction. Appearance of the defined peak at 0.15 V in citrate/chloride electrolyte could be attributed to the dedoping of citrate anions or reduction of the polyaniline degradation products [17]. The main degradation product appears to be soluble benzoquinone with the redox of the benzoquinone/hydroquinone couple. Other insoluble degradation products have been suggested to remain on the electrode surface, including PANI strands containing quinoneimine end groups [18, 19] and ortho-coupled polymers [20].

Figure 3 shows typical charge-discharge curves of polyaniline electrode for the different current densities, in solution contained ammonium-zinc chloride and with addition of the sodium citrate.

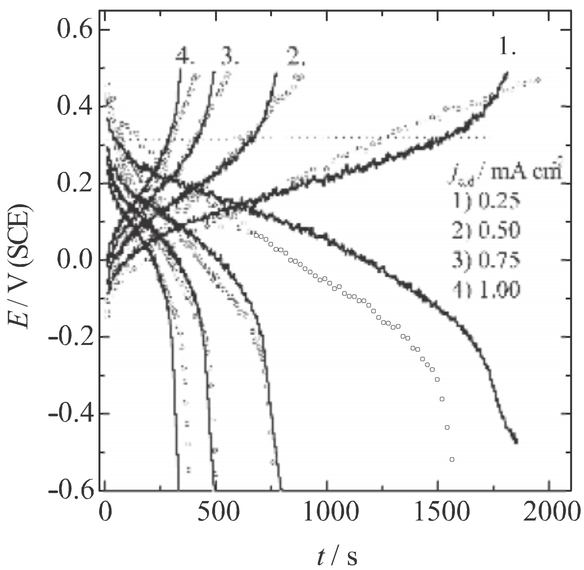

Figure 3 : Charge-discharge curve of the polyaniline electrode in (o) chloride and in ( ) chloride/citrate electrolyte for different current densities.

Charging of the PANI electrode in booth electrolytes starts at potential of ~ –0.1 V. In chloride electrolyte potential increase linearly up to 0.5 V, while in chloride/citrate electrolyte above 0.35 V faster increase of potential is observed (marked with doted line in Figure 3). Such behavior of PANI electrode in chloride/citrate electrolyte could be connected with overcharging of the electrode, most probably with formation of degradation products. Discharge of the electrode occurs in the potential range between ~0.45-0.3 and ~–0.2 V with an average discharge potential of ~0.1 V. Even the chloride electrolyte has higher open circuit potential, chloride/citrate electrolyte shows better discharge characteristics, especially for lower current densities. After potentials more negative than –0.1 V diffusion limitations provoke the sharp decrease of the potential.

On Figure 4 dependence of electrode capacity, during the charge/discharge for different current densities are shown. Charging/discharging characteristics of PANI electrode in both electrolytes are affected with applied current density, probably provoked by anion diffusion limitation through PANI film. Columbic efficiency is much better in chloride/citrate electrolyte than in chloride electrolyte, as it can be seen from the insert of the Figure 4. In the range of investigated current densities of 0.25 to 1 mA cm^{-2}, electrode capacity was in the range of 0.140 to 0.08 mA h cm^{-2} or 140 to 80 mA h g^{-1}, respectively.

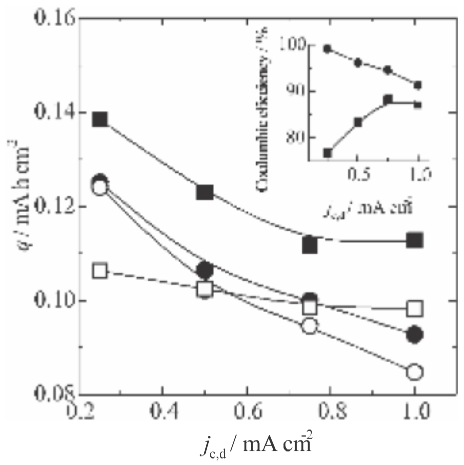

Figure 4 : Dependence of charge/discharge electrode capacity for different current densities of PANI electrode in (o) chloride/citrate and in (□) chloride electrolyte, full symbols charge, open symbols discharge. Insert: Columbic efficiency.

As shown previously, for the anodic potential limit of 0.5 V during cyclization booth electrolyte shows decrease of electrode capacity, but decrease of the capacity was much more pronounced in chloride/citrate electrolyte [21, 22]. Keeping in mind that chloride/citrate electrolyte could have some potential advantages for the negative, zinc, electrode the behavior of the PANI electrode in this electrolyte at a constant current density of 1 mA cm^{-2} versus the cycle number was investigated, and results are shown on Figures 5 and 6. The cycling potentials were limited to 0.50 and 0.32 V for charging and to –0.65 V for discharging.

From the Figures 5 and 6, it is obvious that anodic potential limit has a great influence on cyclic behavior of PANI electrode in the chloride/citrate electrolyte. For the anodic potential limit of 0.5 V (Figure 5), charging/discharging time decrease with increasing number of cycles. On the contrary, for the anodic potential limit of 0.32 V (Figure 6) charging/ discharging time has practically constant value. It is worth to mention that chloride electrolyte (shown with doted line on Figure 6) for the anodic potential limit of 0.32 V has practically only the half of the electrode discharge capacity obtained in chloride/citrate electrolyte.

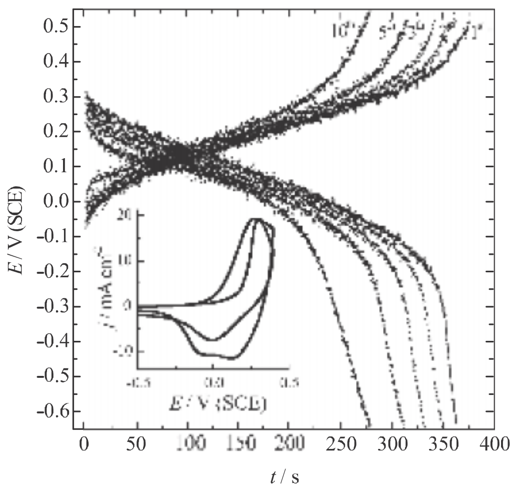

Figure 5 : Charge/discharge curve at a constant current density of 1 mA cm^{-2} versus cycle number in chloride/citrate electrolyte for the anodic potential limit of 0.5 V. Insert: cyclic voltammograms (v=20 mV s^{-1}) of the PANI electrode during cyclization.

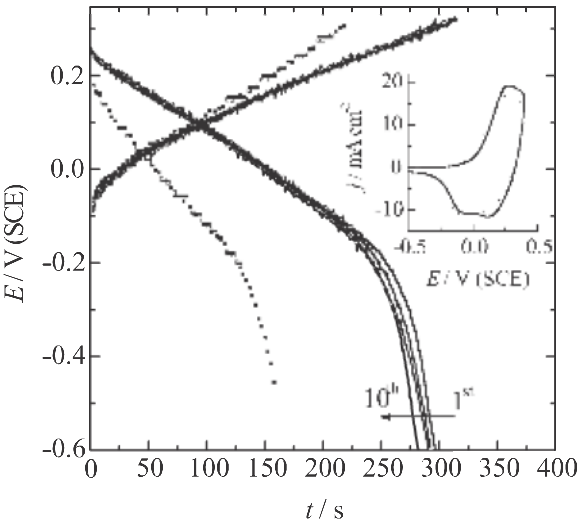

Figure 6 : Charge/discharge curve at a constant current density of 1 mA cm^{-2} versus cycle number in chloride/citrate electrolyte for the anodic potential limit of 0.32 V (doted line-chloride electrolyte). Insert: cyclic voltammograms (v=20 mV s^{-1}) of the PANI electrode during cyclization.

On the inserts of Figures 5 and 6 cyclic voltammograms of the PANI electrode before first and after tenth cycles of the charge/discharge are shown. As it can be seen from insert of Figure 5, for anodic potential limit of 0.5 V cyclic voltammograms shows dramatic changes during cyclization. Comparing the initial voltammograms with one obtained after tenth cycles of charge/discharge it could be concluded that strong degradation of PANI electrode occurred. Hence, it could be suggested that anodic potential limit of 0.5 V during cyclization provoke formation of the inactive, probably lower molecular weight chains, in PANI electrode. At the moment it is impossible to suggest weather this inactivation is connected with formation of soluble or insoluble products. On the contrary, for anodic potential limit of 0.32 V, cyclic voltammograms during cyclization practically remains the same, as it can be seen from the insert of Figure 5, indicating that degradation of PANI practically do not occur.

As the electrode was polymerized at the same conditions, decrease of the capacity with higher anodic potential limit can be connected with presence of citrate anions. The contrary anion effects, as proposed by Yang et al. [23] may be attributed to hydrophobicity of anions, following the Hofmeister series [24]:

$ClO_4^- > NO_3^- > I^- > Br^- > Cl^- > F^- > HPO_4^{2-} > SO_4^{2-} > citrate^{3-}$

Hence, perchlorate ions are the most hydrophobic, citrate ions are the most hydrophilic, while chloride are in the middle. So, chloride anions are expected to form relatively stable ion pairs in the oxidized PANI film, and the PANI degradation may be limited to some degree by the dissociation of the ion pair, resulting in a slower PANI degradation kinetics in chloride than in chloride/citrate containing electrolytes.

Figure 7 shows the cyclic voltammograms of the PPy electrode in different electrolytes. In chloride electrolyte, anodic peak at ~0.1 V and cathodic peak at ~ –0.3 V were well pronounced, while in chloride/citrate electrolyte cathodic peak was not pronounced. It seams that dedoping reaction in chloride/citrate electrolyte occur even at the potentials more negative than –0.8 V. Doping/dedoping reactions in pure citrate electrolyte seams to be limited by the size of citrate anions, and cyclic voltammograms was deformed.

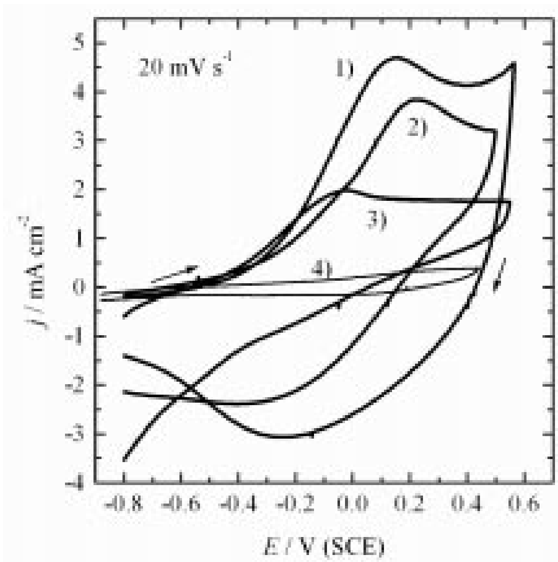

Figure 7 : Comparison of cyclic voltammograms (20 mV s^{-1}) of PPy electrode in 1) chloride, 2) chloride/citrate 3) pure citrate electrolyte and 4) for the bare graphite electrode.

Typical charge-discharge curves of PPy electrode for the different current densities in solution contained ammonium-zinc chloride and with addition of the sodium citrate, are shown on Figure 8.

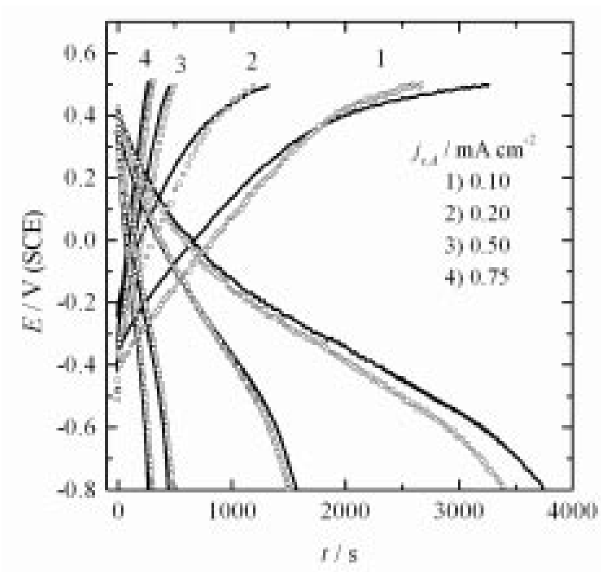

Figure 8 : Charge-discharge curve of the PPy electrode in (o) chloride and in (—) chloride/citrate electrolyte for different current densities.

Charging of the electrode in booth electrolytes starts at potential of ~ –0.5 V, while discharging at potential range between 0.4 to –0.8 V, without stable potential plateaus. It is interesting to note that charge/discharge curves in both electrolytes are very similar. Hence, it could be concluded that citrate anions practically does not have lot of influence on charge/discharge characteristic in chloride/citrate electrolyte.

On Figure 9 dependence of electrode capacity, during the charge/discharge for different current densities are shown. Charging/discharging characteristics of PPy electrode in both electrolytes are affected with applied current density, probably provoked by anion diffusion limitation through film.

For low current densities of 0.1 and 0.2 mA cm^{-2} columbic efficiency was higher than 100%, as it can be seen from the insert of the Figure 9. This could be explained by the possibilities of hydrogen evolution reaction at low current densities at negative potentials. Hence, in the range of investigated current densities of 0.1 to 0.75 mA cm^{-2}, discharge electrode capacity seams to be most probably in the range of 0.075 to 0.045 mA h cm^{-2} or 100 to 60 mA h g^{-1}, respectively.

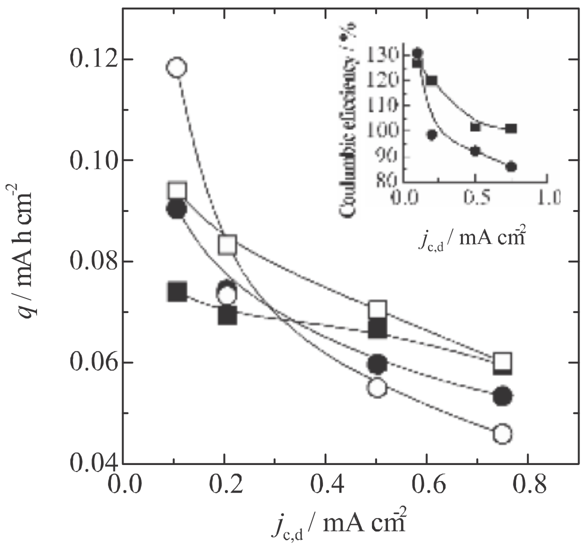

Figure 9 : Dependence of charge/discharge electrode capacity for different current densities of PPy electrode in (o) chloride/citrate and in (□) chloride electrolyte, full symbols charge, open symbols discharge. Insert: Columbic efficiency.

Figure 10 shows the cyclic behavior of the PPy electrode in chloride/citrate electrolyte at a constant current density of 0.5 mA cm^{-2}. The cycling potentials were limited to 0.50 V for charging and to –0.8 V for discharging. As it can be seen, during cyclization electrode capacity slightly increase from 85 to 95 mA h g^{-2}.

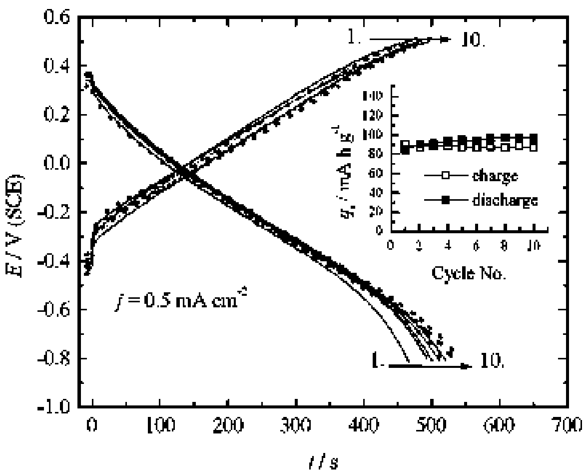

Figure 10 : Charge/discharge curve of PPy electrode at a constant current density of 0.5 mA cm^{-2} versus cycle number in chloride/citrate electrolyte. Insert: obtained specific charge during cyclization.

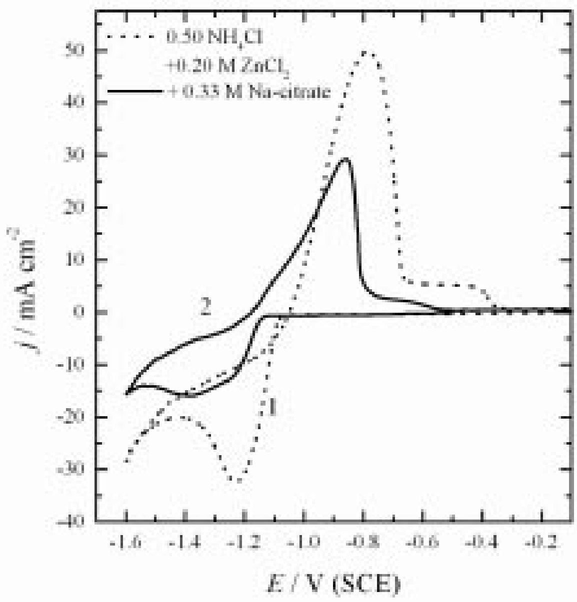

Figure 11 : Cyclic voltammograms of graphite electrode in 1) 0.50 M NH_4Cl + 0.20 M $ZnCl_2$ and 2) with addition of 0.33 M Na-citrate. Sweep rate 20 mV s^{-1}.

3.2. Zinc electrode

Figure 11 shows cyclic voltammograms of zinc deposition-dissolution on graphite electrode in chloride and chloride/citrate containing electrolytes. As it can be seen from chloride electrolyte deposition processes start at potentials around –1 V, thought one well defined peak with the maximum at –1.17 V. At potentials more negative than –1.4 V proceed simultaneous zinc deposition and hydrogen evolution reactions. In anodic direction, zinc dissolution occurs at potentials more positive than –1 V through one pack and one shoulder. In citrate/chloride electrolyte deposition-dissolution reaction is shifted for ~0.15 V in negative direction and diffusion limited peak is approximately two times smaller, than in chloride electrolytes. This behavior could be explained by zinc ions complexation and lowering the free zinc ions activity, as well as diffusivity of zinc citrate complex comparing with chloride electrolyte.

Slow potentiodinamic (v=1 mV s^{-1}) polarization curves in chloride and chloride/citrate electrolyte on solid zinc electrode are shown on Figure 12. Open circuit potential, E_{ocp}, of zinc electrode assuming reactions:

$$Zn = Zn^{2+} + 2e \text{ (chloride electrolyte)} \quad (2)$$

and

$$Zn + cit^{3-} = [Zn\ cit]^{-} + 2e \quad (3)$$

(chloride/citrate electrolyte)

in chloride electrolyte where –0.997 V which was ~130 mV more positive than in chloride/citrate electrolyte, E_{ocp}= – 1.125 V. In ideal case without corrosion, E_{ocp} can be attributed to reversible electrode potentials.

Determined Tafel slopes for the chloride electrolyte were ± 33 mV dec^{-1}, and exchange current density, extrapolated from intercept of Tafel lines with open circuit potentials was 1.02 mA cm^{-2}. Those kinetic parameters suggest diffusion control of deposition and dissolution reaction. In the chloride/

citrate electrolyte anodic Tafel slope was –33 mV dec^{-1}, while cathodic Tafel slope was –30 mV dec^{-1}, at low current densities and not well define slope of –125 mV dec^{-1} at high current density, respectively. Determined exchange current density of 0.076 mA cm^{-2}, was more than one order of magnitude smaller then in chloride electrolyte. Hence, it should be expected that in chloride/citrate electrolyte corrosion of zinc electrode should be smaller than in chloride electrolyte.

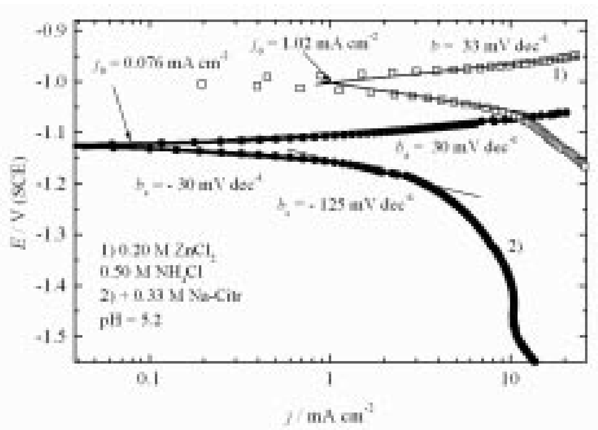

Figure 12 : Slow potentiodinamic (IR corrected) polarization curve (v=1 mV s^{-1}) in chloride (1) and chloride/citrate (2) electrolyte on solid zinc electrode.

On Figure 13, galvanostatic charge/discharge curve of zinc electrode for different current densities in chloride and chloride/citrate electrolyte are shown. In chloride electrolyte, practically no differences between different current densities can be seen, mainly due to the very fast reaction and low values of Tafel slopes. In chloride/citrate electrolyte, discharging curve is not affected with applied current densities, mainly due to the similar Tafel slope as in chloride solution. On the contrary, charging curves are affected with applied current densities, due to the higher Tafel slope in that current density region, and diffusion limitations which occur at current densities above 8 mA cm^{-2}. Relatively small current densities for charging reactions of zinc electrode in citrate containing electrolyte can be further increase with increasing zinc chloride and sodium citrate concentrations.

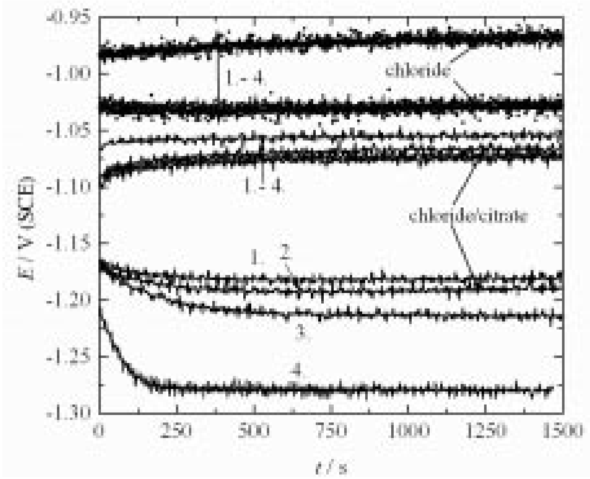

Figure 13 : Charge/discharge characteristic of the zinc electrode in chloride and in chloride citrate electrolyte at the current densities of: 1) 2.25, 2) 3.0, 3) 5,0 and 4) 8.0 mA cm^{-2}.

Figure 14 shows micrographs of zinc deposits on copper substrate obtained from chloride and chloride/citrate electrolytes at a constant current density of 3.5 mA cm^{-2} and with deposition charges of 10.5 mA h cm^{-2}.

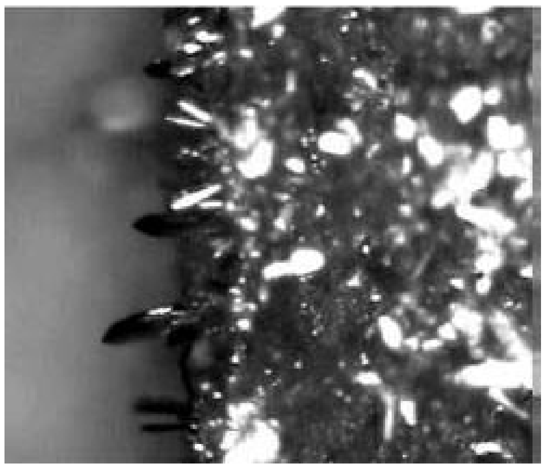

(a)

Figure 14 : Micrographs of the zinc deposits from a, c) 0.20 M $ZnCl_2$ + 0.50 M NH_4Cl and b, d) with addition of 0.33 M Na-citrate. Deposition current density 3.5 mA cm^{-2}, deposition time 3 h, magnification 200 x.

(b)

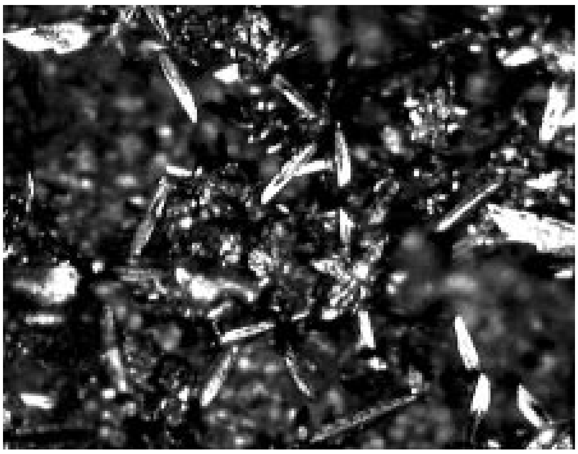

(c)

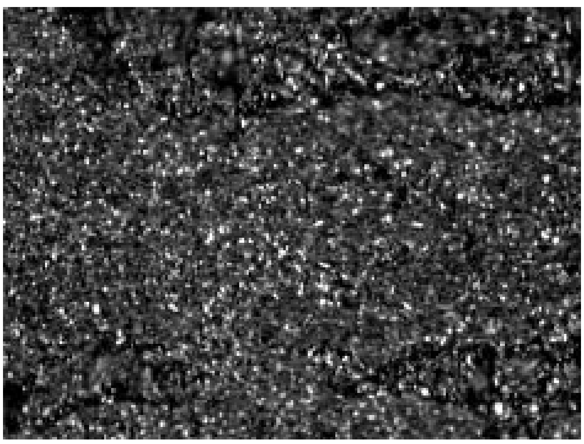

(d)

In chloride electrolyte, Figure 14a and c, obtained deposits are practically completely dendritic, even at the relatively low current densities of 3.5 mA cm^{-2} which corresponds to the middle of Tafel slope. So, potential risk of fast dendrite growth through separator, during the longer charging times, and formation of short circuits with cathode is permanently present. On the other hand, in chloride/citrate electrolyte, Figure 14b and d, deposit is smooth without irregularities even in the edges (Fig 14b) where local current density due to the current distribution phenomena is higher than at the central surface. Such differences can be explained in the following way.

The classical expression for the steady state nucleation rate, J, is given by [12]:

$$J = K_1 \exp\left(\frac{K_2}{\eta^2}\right) \qquad (4)$$

where K_1 and K_2 are overpotential, h, (h=E – E_{ocp}) independent constants. Equation (4) is valid for a number of systems regardless of the value of the exchange current density for the deposition process. At one and the same deposition current density, j, decreasing j_0 leads to an increasing nucleation rate and decreasing nucleation exclusion zones radii [12]. The saturation nucleus density, i.e., the exchange current density of the deposition process, strongly affects the morphology of metal deposits. At high exchange current densities, the radii of the screening zones are large and the saturation nucleus density is low. This permits the formation of large, well-defined crystal grains and granular (dendrite) growth of the deposit. At low exchange current densities, the screening zones radii are low, or equal to zero, the nucleation rate is large and a smooth deposit can be easily formed.

The nucleation law can be written as:

$$N = N_0\left[1 - \exp(-At)\right] \qquad (5)$$

where

$$A = K_1 j_0 \exp\left(-\frac{K_2}{\eta^2}\right) \qquad (6)$$

and N_0 is the saturation nucleus surface density (nuclei cm^{-2}), being dependent on the exchange current density of deposition process and the deposition overpotential. The overpotential and the current density in activation-controlled deposition inside the Tafel region are related by:

$$\eta = \frac{b_c}{2.3} \ln \frac{j}{j_0} \qquad (7)$$

Therefore, increasing b_c and decreasing j_0 leads to an increase in the deposition overpotential at the constant current density. According to Eq. 6, the value of A increases with increasing overpotential and decreases with decreasing exchange current density. It follows from all available data that the former effect is more pronounced resulting in deposits with a finer grain size with decreasing value of the exchange current density.

This analysis explain differences in deposit morphology for chloride and chloride/citrate electrolytes taking into account that Tafel slopes for deposition reaction are –33 and –125 mV dec^{-1}, and exchange current density are 1.02 and 0.078 mA cm^{-2}, respectively. Hence, in chloride electrolyte at 3.5 mA cm^{-2} deposition overpotential is only 25 mV, while in chloride/citrate electrolyte is more than 80 mV.

Considering obtained results for the PANI, PPy and zinc electrode, Fig 15 shows possible characteristics of Zn|PANI and Zn|PPy cells in chloride/citrate electrolyte, at the anodic current densities of 5 mA cm^{-2} and cathodic current densities of 0.5 mA cm^{-2}. It was assumed that with development of PANI or PPy electrode on high surface area support, 0.5 mA cm^{-2} of flat surface corresponds to approximately 5 mA cm^{-2} on high surface area support.

As it can be seen from the Fig 15, for the same synthesis and operating conditions PANI electrode shows much better electrochemical characteristic than PPy electrode.

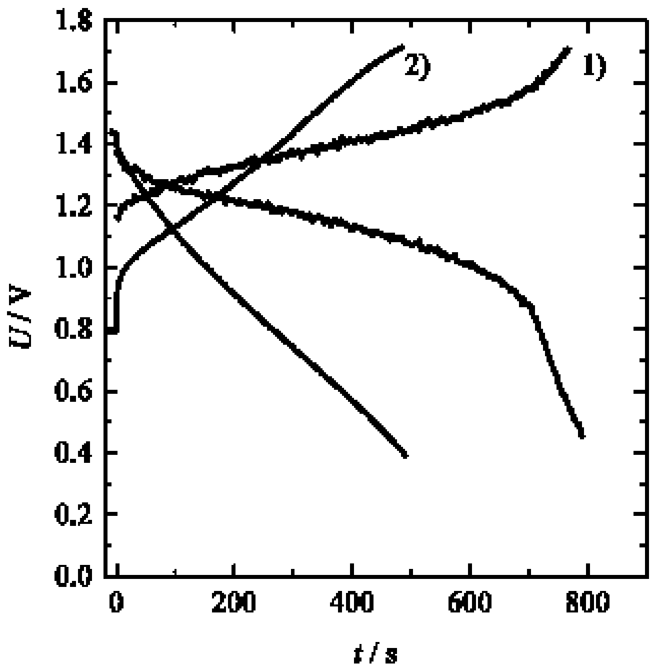

Figure 15 : Possible characteristics of 1) Zn|PANI and 2) Zn|PPy cells in chloride/citrate electrolyte.

CONCLUSIONS

Based on the presented results it has been concluded that chloride/citrate electrolyte have some potential advantages in comparison with chloride electrolytes for zinc-PANI secondary cells. Citrate anions due to the complexation of free zinc ions produce negative shift of the open circuit potentials for ~ 130 mV. On the other hand, decrease of exchange current density and increase of Tafel slope lower dendrite formation and zinc corrosion rate. In cycling regime citrate/chloride electrolytes shows better characteristic (higher specific capacity and columbic efficiency) for anodic potential limit of 0.32 V (SCE), then chloride electrolyte. Faster decrease of specific capacity in cycling regime for anodic potential limits of 0.5 V (SCE) in chloride/citrate than in chloride electrolyte has been explained by higher hydrophilic effect of citrate anions.

For the same synthesis and operating conditions PANI electrode shows much better electrochemical characteristic than PPy electrode.

ACKNOWLEDGMENT

This work is financially supported by the Ministry of Science and Environmental Protection, Republic of Serbia, contract No. 142044. Author is grateful to Mr. Branimir Jugoviæ and Dr. Milica Gvozdenoviæ for useful helps.

REFERENCES

1. R. de Surville, M. Josefowicz, L.T. Yu, J. Perichon and R. Buvet. Electrochi. Acta 13, (1968), P 1451.
2. M. Kaya, A. Kitani, K. Sasaki, Denki Kagaku 52, 1984, P 847.
3. A. Kitani, M. Kaya and K. Sasaki, J. Elecrochem. Soc. 133, 1986, P 1069.
4. 1. M. Sima, T. Visan, M. Buda, J. Pow. Sourc. 56, 1995, P 133.
5. A. Mirmohseni, R. Solhjo, European Polymer Journal 39, 2003, P 219.
6. F. Trinidad, M.C. Montemayor and E. Fatas. J. Electrochem. Soc. 138, 1991, P 31863
7. L.D Arsov, W. Plieth, G Kossmehl, J. Solid State Electrochem. 6, 1998, P 355.
8. H. N. Dinh, J. Ding, S.J. Xia, V. I. Birss, J. Electroanal. Chem 459, 1998, P 45.
9. J. Kan, H. Xue, S. Mu . J. Pow. Sources 74, 1998, P 113.
10. G. Mengoli, M.M. Musiani, D. Pletcher, S. Valcher, J. Appl. Electrochem. 17, 1987, P 515.
11. M.S. Rahmanifar, M.F. Mousavi, M. Shamsipur, M. Ghaemia, J. Pow. Sources 132, 2004, P 296.
12. K. I. Popov, S. S. Đokic, B. N. Grgur, Fundamental Aspects of Electrometallurgy, Kluwer Academic/Plenum Publishers, New York, 2002.
13. E. Erdem, M. Saçak, M. Karakiºla, Polymer International 39, 1996, P 153.
14. J. Kankare, in: D. Wise, G.E. Wnek, D.J. Trantolo, T.M. Cooper, J.D. Gresser (Eds.), Electrical and Optical Polymer Systems: Fundamentals, Methods, and Applications, Marcel Dekker, New York, 1998, Ch.6.
15. M.M. Popoviæ, B.N. Grgur, Synt. Met. 143, 2004, P 191.
16. N. Gospodinova, L. Terlemezyan, Prog. Polym. Sci. 23, 1998, P 1443.
17. H. N. Dinh, J. Ding, S.J. Xia, V. I. Birss, J. Electroanal. Chem. 459, 1998, P 45.
18. D.E. Stilwell, S-M Park, J. Electrochem. Soc. 135, 1988, P 2491.
19. D.E. Stilwell, S.-M. Park, J Electrochem. Soc. 135, 1988, P 2497.

20. A.Q. Zhang, C.Q. Cui, J.Y. Lee, Synt. Met. 72, 1995, P 217.

21. 13. B.Z. Jugoviæ, T. Lj. Trišoviæ, J.S. Stevanoviæ, M.D. Maksimoviæ, B.N. Grgur, Electrochim. Acta 51, 2006, P 6268.

22. B.Z. Jugoviæ, T. Lj. Trišoviæ, J.S. Stevanoviæ, M.D. Maksimoviæ, B.N. Grgur, J. Pow. Sourc. 160, 2006, P 1447.

23. X. Yang, Q. Xie., S. Yao, Synth. Met. 143, 2004, P 119.

24. W. Kunz, J. Henle, B. W. Ninham, Curr. Opin. Coll. Interface Sci. 9, 2004, P 19.